IOTA Technical Report
Signal-To-Noise Ratio of Interference Fringe Parameters

R. Millan-Gabet[a], F. P. Schloerb[a], W. A. Traub[b] and H. M. Dyck[c]

[a]Physics and Astronomy Department
University of Massachusetts at Amherst
Amherst, MA 01003, USA

[b]Smithsonian Astrophysical Observatory
60 Garden St., Cambridge, MA 02138, USA

[c]Department of Physics and Astronomy
University of Wyoming
Laramie, WY 82071, USA

April, 6, 1995

ABSTRACT

We develop analytical expressions for the signal-to-noise-ratio of interference fringe parameters. The techniques of delay modulation and dispersed fringes are considered. We examine different possible types of detectors for fringe detection in the infrared at the Infrared Optical Telescope Array (IOTA) and apply our formalism to the measurement of fringe visibility in the optical and infrared.

1. INTRODUCTION

The essence of astronomical Michelson interferometry lies in the determination of the structure of a source through measurement of the coherence properties of its optical field. The importance of the technique lies in its ability to provide such information at an angular resolution $\sim \lambda/B_{max}$, where B_{max} is the baseline vector given by the maximum separation of the telescopes. Moreover, the technique can be made insensitive to atmospheric turbulence provided that we use apertures of size D smaller than the atmospheric coherence length (r_0) and freeze the fluctuations of the phase of the fields by detecting interference fringes in a time shorter than the atmospheric coherence time (τ_0). The coherence properties may be determined from measurable parameters of the interference fringes and it is therefore important to examine the limitations to fringe parameter measurements. In this paper we consider alternative methods for measuring interference fringes and develop simple analytical formulas that we can use as a basis for studying the dependence of the signal to noise ratio (SNR) on the different parameters involved in the problem. Although the Infrared-Optical Telescope Array (IOTA)[1] has been producing scientific results since December 1994, presently our group has among its main priorities the determination of the optimum detection techniques for both our optical and infrared experiments. This effort will translate into the design and implementation of IOTA's second generation detection schemes and instrumentation, thus improving the interferometer's present sensitivity limits and expanding the class of astronomical problems accesible. The work presented here is intended to provide a basis for quantitative comparison between the expected performance of the different possible techniques and detectors available to us.

Other author information: (Send correspondence to R.M.G.)
E-mail: rmillang@comet.phast.umass.edu

2. RESPONSE OF THE INTERFEROMETER

In a two-telescope interferometer the incoming wavefront is spatially sampled by apertures 1 and 2, and after propagation through the instrument and introduction of a delay between the two arms, the fields are re-combined at a beam splitter. The intensity incident on the detector at the focal plane of the instrument can then be written as:

$$R(u,v,\nu,\tau) = I_0(1 + Re\{\gamma_{1,2}(\tau)\}) \tag{1}$$

where $\gamma_{1,2}(\tau)$ is the *complex degree of coherence*, a measure of the temporal and spatial coherence properties of the sampled fields; $I_0(\nu)$ represents the incident intensity (from both apertures, after propagation through the instrument, assuming equal contributions from each arm and one beam splitter output); τ is the sum of the delay due to the source-baseline geometry and the instrumental delay; ν is the optical frequency and (u,v) are the components (in wavelengths) of the baseline vector projected on the sky.

The complex degree of coherence in equation (1) is related via a double Fourier transformation to both the spectral and spatial structure of the source. The ultimate goal of interferometric methods is to extract that information from measurement of the coherence function via measurement of interference fringes.

The complex degree of coherence may either be measured by detecting interference fringes in wavenumber or delay space. In the *dispersed fringes* technique, the delay is kept constant and, following beam combination, the light is spectrally dispersed across an array detector producing a frequency modulation of the response. In the *delay fringes* technique, all light within the spectral bandpass is integrated and a single pixel may be used to detect the fringe modulation produced by scanning the delay on either side of the white light fringe (WLF, given by the condition $\tau = 0$). In this case we insure probing only spatial coherence by measuring the contrast of the fringes near zero optical path difference.

We can conveniently visualize each of those measurement processes with the aid of the following diagrams. In Figures 1 and 2, each dot represents a photon incident on the detector and the strips indicate the range in time and frequency involved in the measurement.

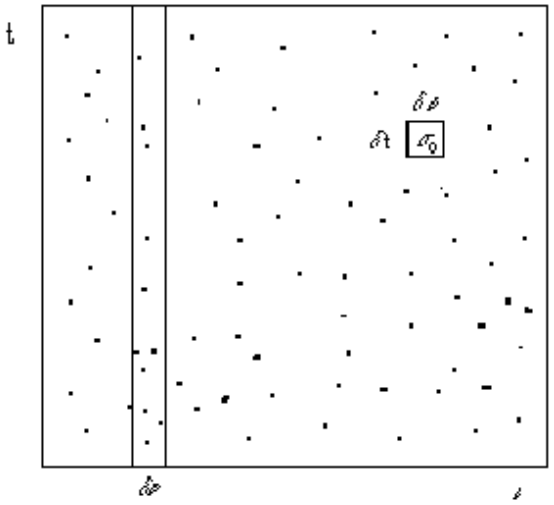

Figure 1. Dispersed fringes. In this case we denote the spectral width corresponding to each pixel (the spectral resolution) by $\delta\nu$. The integration time is limited by the atmospheric coherence time (τ_0) so that the fringe contains the atmospheric phase errors frozen in it. For this illustration, we adopt an integration time equal to the atmospheric coherence time. The number M of data points in the fringe satisfies $M = 2\Delta\nu/\delta\nu$, where $\Delta\nu$ is the spectral half-width of the radiation detected.

In order to calculate the response of the interferometer in each detection mode, let us consider first the monochromatic limit. In that case the complex degree of coherence and the brightness distribution of a spatially incoherent

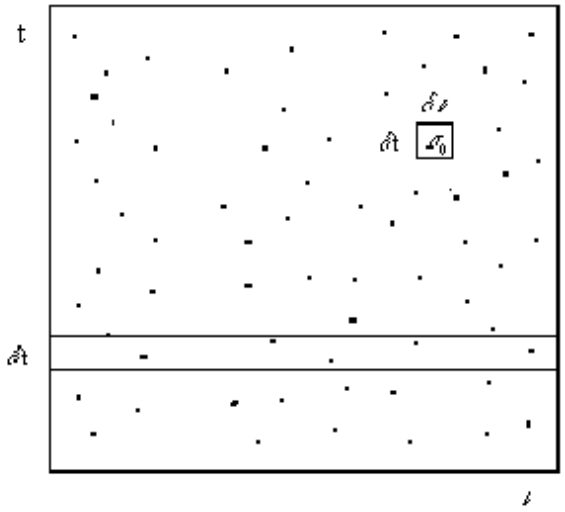

Figure 2. Delay fringes. In this case we denote by δt the integration time corresponding to one detection bin. If the number of data points in the fringe is M, we must have $M = \tau_0/\delta t$, where the total time in the fringe is again limited by the atmosphere by the necessity to preserve the phase relationship between the first and last data points and is taken to be equal to τ_0.

source in the far field of the interferometer form a Fourier transform pair. In the usual terminology of astronomy, the complex degree of coherence is then the normalized *visibility function* $\overline{V}(u,v)$. If we denote its modulus by $\overline{V}$ and its phase by Φ_V then, allowing for a Gaussian spectral intensity filter centered at ν_0 and of $1/e-$half width $\Delta\nu$, the fringe pattern may be described by:

$$R(u,v,\nu,\tau) = I_0 e^{-(\nu-\nu_0)^2/\Delta\nu^2}[1+\overline{V}\cos(2\pi\tau\nu-(\Phi_V+\Phi_a+\Phi_i))] \tag{2}$$

where the fringe phase is the sum of the phase of the visibility function (Φ_V), the phase distorsion introduced by propagation through the turbulent atmosphere (Φ_a, a random variable) and a phase term due to instrumental aberrations (Φ_i). Thus, the components of the visibility function may then be determined from measurement of the fringe contrast and the fringe phase with respect to $\tau = 0$. The subsequent process of recovery of the source brightness distribution is limited by the finite sampling of the visibility function, the ability to extract the phase of the visibility function from the fringe phase and the accuracy of the fringe parameter measurements.

Considering the monochromatic response and the measurement processes described by figures 1 and 2, we can now write the interference patterns in terms of the number of photons detected as a function of frequency or delay as:

$$K(\nu) = \eta\int_{\nu-\delta\nu/2}^{\nu+\delta\nu/2}\int_{\tau_0} R d\nu dt, \text{ for dispersed fringes} \tag{3}$$

$$K(\tau) = \eta\int_{\nu_0-\Delta\nu}^{\nu_0+\Delta\nu}\int_{\tau-\delta t/2}^{\tau+\delta t/2} R d\nu dt, \text{ for delay fringes} \tag{4}$$

where η is the detector quantum efficiency.

We expect both techniques to result in identical predictions for the SNR of the fringe parameters since in both cases the same amount of information is present.

3. DISPERSED FRINGE RESPONSE

We detect the dispersed fringes across an array of M pixels. Considering equation (3) and assuming that the response is approximately constant for the range of frequency corresponding to one pixel ($\delta\nu$) and during the integration time (τ_0), we may model the response as:

$$K(\nu_i) = e^{-(\nu_i-\nu_0)^2/\Delta\nu^2}.(a + b\cos(2\pi\nu_i\Psi - \Phi)), i = 1, ..., M \tag{5}$$

where ν_i is the center frequency for each pixel and, aside from the Gaussian modulation, a represents the average number of photons detected per pixel; b is proportional to the modulus of the normalized visibility function and Ψ is the offset with respect to the WLF. We have assumed that the source is gray within the bandpass.

Denoting the model parameters by $(a_0, b_0, \Psi_0, \Phi_0)$, we can linearize the above response in the fringe parameters $(a, b, \Delta\Psi, \Delta\Phi)$, the last two parameters being the phase corrections required to fit the fringe. Using linear least squares fitting, gives then the best estimates of the fringe parameters:

$$a = \frac{\sum_{i=1}^{M} K_i.e^{-(\nu_i-\nu_0)^2/\Delta\nu^2}}{\sum_{i=1}^{M} e^{-2(\nu_i-\nu_0)^2/\Delta\nu^2}} \tag{6}$$

$$b = \frac{2\sum_{i=1}^{M} K_i.e^{-(\nu_i-\nu_0)^2/\Delta\nu^2}.\cos(2\pi\nu_i\Psi_0 - \Phi_0)}{\sum_{i=1}^{M} e^{-2(\nu_i-\nu_0)^2/\Delta\nu^2}} \tag{7}$$

$$\Delta\Psi = \frac{-\sum_{i=1}^{M} K_i.\nu_i.e^{-(\nu_i-\nu_0)^2/\Delta\nu^2}\sin(2\pi\nu_i\Psi_0 - \Phi_0)}{\pi b_0 \sum_{i=1}^{M} \nu_i^2.e^{-2(\nu_i-\nu_0)^2/\Delta\nu^2}} \tag{8}$$

$$\Delta\Phi = \frac{2\sum_{i=1}^{M} K_i.e^{-(\nu_i-\nu_0)^2/\Delta\nu^2}\sin(2\pi\nu_i\Psi_0 - \Phi_0)}{b_0 \sum_{i=1}^{M} e^{-2(\nu_i-\nu_0)^2/\Delta\nu^2}} \tag{9}$$

and their variances:

$$\sigma_a^2 = \sigma^2 \frac{1}{\sum_{i=1}^{M} e^{-2(\nu_i-\nu_0)^2/\Delta\nu^2}} \tag{10}$$

$$\sigma_b^2 = \sigma^2 \frac{2}{\sum_{i=1}^{M} e^{-2(\nu_i-\nu_0)^2/\Delta\nu^2}} \tag{11}$$

$$\sigma_{\Delta\Psi}^2 = \sigma^2 \frac{1}{2\pi^2 b_0^2 . \sum_{i=1}^{M} \nu_i^2.e^{-2(\nu_i-\nu_0)^2/\Delta\nu^2}} \tag{12}$$

$$\sigma_{\Delta\Phi}^2 = \sigma^2 \frac{2}{b_0^2 . \sum_{i=1}^{M} e^{-2(\nu_i-\nu_0)^2/\Delta\nu^2}} \tag{13}$$

where σ represents the error in the data in a single bin and we assume that it is the same for all data points.*

A good approximation to the sums appearing in the parameter variances can be obtained by replacing them by appropriate integrals. Assuming that the M data points lie within the $1/e-$full width ($2\Delta\nu$) of the spectral envelope, it is a straightforward calculation to show that:

$$\sigma_a^2 = \sigma^2 \frac{1}{\alpha\sqrt{2\pi}} \frac{2}{M} \tag{14}$$

*This is a good assumption if the error in the data is dominated by detector noise. If on the contrary, the main source of error is photon noise, the assumption is clearly not valid. It has been shown by Traub (private communication) that the error in the fringe visibility (V) obtained by fitting Poisson weighted data instead of uniformly weighted data is about a factor of 3 lower for V=1. For V $\leq$ 0.5 the results differ by only a factor of $\sim$ 1.1.

$$\sigma_b^2 = \sigma^2 \frac{2}{\alpha\sqrt{2\pi}} \frac{2}{M} \quad (15)$$

$$\sigma_{\Delta\Psi}^2 = \frac{\sigma^2}{\pi^2 b_0^2} \frac{1}{\left[\left(\frac{\Delta\nu}{2}\right)^2 \beta + \nu_0^2 \sqrt{2\pi}\alpha\right]} \frac{1}{M} \quad (16)$$

$$\sigma_{\Delta\Phi}^2 = \frac{\sigma^2}{b_0^2} \frac{2}{\alpha\sqrt{2\pi}} \frac{2}{M} \quad (17)$$

where α is related to the error function associated with the normal distribution by: $\alpha = \frac{1}{2} erf(\sqrt{2}) = 0.48$ and β is given by: $\beta = \int_0^2 z^2 e^{-z^2/2} dz = 0.93$.

4. DELAY FRINGE RESPONSE

In this case we detect the fringe in a single pixel and the whole bandpass is integrated in each data bin. Considering equation (4) and assuming that the response is approximately constant for the short range in delay corresponding to one data bin (δt), we may model the response as:

$$K(\tau_i) = a' + b'.e^{-\pi^2(\tau_i - \Psi')^2 \Delta\nu^2}.\cos(2\pi(\tau_i - \Psi')\nu_0 - \Phi), i = 1, ..., M \quad (18)$$

where, similarly to the previous case, τ_i is the center delay for each data bin; a' represents the average number of detected photons per bin; b' is proportional to the modulus of the normalized visibility function and Ψ' represents the geometrical delay corresponding to the WLF. We have again assumed a gray source within the bandpass.

Using an identical procedure as before, we linearize the above expression in the fringe parameters $(a', b', \Delta\Psi', \Delta\Phi)$. Fitting, then, gives us the best estimates:

$$a' = \frac{1}{M} \sum_{i=1}^{M} K_i \quad (19)$$

$$b' = \frac{2\sum_{i=1}^{M} K_i.e^{-\pi^2(\tau_i - \Psi_0')^2 \Delta\nu^2}.\cos(2\pi(\tau_i - \Psi')\nu_0 - \Phi_0)}{\sum_{i=1}^{M} e^{-2\pi^2(\tau_i - \Psi_0)^2 \Delta\nu^2}} \quad (20)$$

$$\Delta\Psi' = \frac{\sum_{i=1}^{M} K_i e^{-\pi^2(\tau_i - \Psi_0')^2 \Delta\nu^2}[\pi\Delta\nu^2(\tau_i - \Psi_0')\cos(2\pi(\tau_i - \Psi_0')\nu_0 - \Phi_0) + \nu_0 \sin(2\pi(\tau_i - \Psi_0')\nu_0 - \Phi_0)]}{\pi b_0' \sum_{i=1}^{M} e^{-2\pi^2(\tau_i - \Psi_0')^2 \Delta\nu^2}[\pi^2\Delta\nu^4(\tau_i - \Psi_0')^2 + \nu_0^2]} \quad (21)$$

$$\Delta\Phi = \frac{2\sum_{i=1}^{M} K_i.e^{-\pi^2(\tau_i - \Psi_0')^2 \Delta\nu^2}.\sin(2\pi(\tau_i - \Psi_0')\nu_0 - \Phi_0)}{b_0' \sum_{i=1}^{M} e^{-2\pi^2(\tau_i - \Psi_0')^2 \Delta\nu^2}} \quad (22)$$

and their variances:

$$\sigma_{a'}^2 = \sigma'^2 \frac{1}{M} \quad (23)$$

$$\sigma_{b'}^2 = \sigma'^2 \frac{2}{\sum_{i=1}^{M} e^{-2\pi^2(\tau_i - \Psi_0')^2 \Delta\nu^2}} \quad (24)$$

$$\sigma_{\Delta\Psi'}^2 = \sigma'^2 \frac{1}{2\pi^2 b_0'^2 \sum_{i=1}^{M} e^{-2\pi^2(\tau_i - \Psi_0')^2 \Delta\nu^2}[\pi^2\Delta\nu^4(\tau_i - \Psi_0')^2 + \nu_0^2]} \quad (25)$$

$$\sigma_{\Delta\Phi}^2 = \sigma'^2 \frac{2}{b_0'^2 \sum_{i=1}^{M} e^{-2\pi^2(\tau_i - \Psi_0')^2 \Delta\nu^2}} \quad (26)$$

where σ' is the error associated with each data point in this case.

If we now assume that the M data points lie within the 1/e-full width of the fringe envelope $(2/\pi\Delta\nu)$, we obtain:

$$\sigma^2_{b'} = \sigma'^2 \frac{2}{\alpha\sqrt{2\pi}} \frac{2}{M} \tag{27}$$

$$\sigma^2_{\Delta\Psi'} = \frac{\sigma'^2}{\pi^2 b_0'^2} \frac{1}{\left[\left(\frac{\Delta\nu}{2}\right)^2 \beta + \nu_0^2 \sqrt{2\pi}\alpha\right]} \frac{1}{M} \tag{28}$$

$$\sigma^2_{\Delta\Phi} = \frac{\sigma'^2}{b_0'^2} \frac{2}{\alpha\sqrt{2\pi}} \frac{2}{M} \tag{29}$$

where the constants α and β have been defined in the previous section.

5. SNR FOR MEASUREMENT OF VISIBILITY AMPLITUDE

We have obtained in sections 3 and 4 variances for the fringe parameters that are identical in form. Moreover, the relationship between the two measurement processes is such that the corrresponding SNRs for the four parameters will be the same as long as the average number of photons detected per bin is the same, as is readily seen by inspection of figures 1 and 2. This fact reflects the fundamental equivalence between the two techniques.

Although the formalism presented in the previous sections would allow us to calculate the SNR for any of the fringe parameters in both our optical and infrared experiments, in this paper we present our results for estimation of the fringe visibility only. Note however the result given by the previous analysis that the uncertainty (in radians) in the determination of the fringe phase is the inverse of the SNR of fringe visibility: $\sigma^2_{\Delta\Phi} = 1/SNR_b$. This provides a simple way of estimating a lower limit for the error in the measurement of fringe position, since the practical limitation in the measurement of this parameter depends on the accuracy with which a reference position is known.

IOTA will ultimately have three telescopes and true imaging using the techniques of phase closure will be possible. We are also currently exploring the potential of techniques for high resolution imaging with only two telescopes.[2] High quality interference fringes and accurate measurements of fringe visibility are crucial to any of those techniques as well as to our present operation mode of parametric imaging using fringe visibilities. Also, these calculations will enable us to establish the quality of our present infrared experiment by comparing the predictions of these calculations with the measured SNRs.

Given the previous results and assuming that the relative error in the determination of the average intensity level in the interferograms is negligible compared to the error in the measurement of the fringe amplitude, we can write the SNR in the determination of the modulus of the normalized visibility function as:

$$\mathrm{SNR}_{\overline{V}} = \left(\frac{\alpha\sqrt{2\pi}}{4}\right)^{1/2} \sqrt{M}.\frac{\overline{K}_S}{\sigma}.\overline{V} \tag{30}$$

where (in a notation now aplicable to either mode of operation) $\overline{K}_S$ is the average number of photons detected in a measurement bin and σ is the error associated with such measurement.

In writing equations (5) or (18) for the response, it is implicit that contributions from the background and detector dark current can be subtracted from the detected signal, and we assume such correction to be ideal. However, the statistical fluctuations of those signals remain and we must express the noise term σ as the quadrature sum of source, background and detector shot noises:

$$\sigma = \sqrt{\overline{K}_S + \overline{K}_B + \overline{K}_D} \tag{31}$$

where $\overline{K}_B$ and $\overline{K}_D$ represent the average number of photocounts per bin from the background and detector noise respectively.

We therefore obtain our final expression:

$$\mathrm{SNR}_{\overline{V}} = \left(\frac{\alpha\sqrt{2\pi}}{4}\right)^{1/2} \frac{\sqrt{M}.\overline{K}_S}{\sqrt{(\overline{K}_S)+(\overline{K}_B)+(\overline{K}_D)}}\overline{V} \tag{32}$$

This equation enables us to evaluate $SNR_{\overline{V}}$ as a function of source magnitude, the parameters involved in the detection arrangement used and detector characteristics. We now proceed to express the quantities involved so as to explicitely show such dependencies. It should be noted that the fringe visibility in the above expression can be factored as the product of the object's true visibility and the intrumental coherence transfer function: $\overline{V} = \overline{V}_{inst}.\overline{V}_{object}$. In this paper however, we are interested in the performance of different devices as fringe detectors. We will therefore ignore the degradation of the quality of the interfering wavefronts by the interferometer optics and by the effects of propagation through the turbulent atmosphere and assume 100% instrumental visibility.

6. APPLICATION TO THE INFRARED EXPERIMENT

We presently operate our infrared experiment using the delay modulation technique, integrating the K-band bandpass in a single detector. In this section we examine the performance of our current detection scheme and the expected performance of our proposed instrumental upgrades.

6.1. Noise Sources

6.1.1. Source Photon Noise

Source photocounts constitutes our signal and the shot noise associated with the statistical fluctuations of this quantity add to the noise of same origin due to photocounts from the background.

Using a standard K-band flux calibration ($F_o = 4.2x10^{-14} W.cm^{-2}.\mu m^{-1}$) and considering the size of each telescope at the IOTA, $D = 45cm$ (roughly equal to the atmospheric coherence length at K); a standard K filter centered at $\lambda = 2.2\mu m$ and $\Delta\lambda = 18\%$ full-width at half maximum and an system optical efficiency of $OE \simeq 0.5$, we readily obtain for the source photocounts from either beam splitter output as a function of the K-band magnitude:

$$\begin{aligned} \overline{K}_S &= F_o.OE.\Delta\lambda_{\mu m}.\frac{1}{2}.\frac{\pi}{4}.D^2_{cm}\left(\frac{\lambda}{hc}\right)_{MKS}.10^{\frac{-mk}{2.5}}\eta.\delta t \\ &= 1.5X10^8 10^{\frac{-mk}{2.5}}\eta\delta t \end{aligned} \tag{33}$$

where η is the detector quantum efficiency and δt is the integration time corresponding to one data point.

6.1.2. Background Noise

Integrating the blackbody emission at 293^oK in the K-bandpass we obtain for the background photocounts:

$$\begin{aligned} \overline{K}_B &= A.\Omega.SE.\left(\frac{\lambda}{hc}\right).\eta.\delta t\int_K \frac{2\pi c^2 h}{\lambda^5}\frac{d\lambda}{\left(e^{\frac{hc}{\lambda KT}}-1\right)} \\ &= 9.2X10^4\eta\delta t \end{aligned} \tag{34}$$

were we have used a detector area-solid angle product $A\Omega = 4\lambda^2$ (a factor of 4 oversized with respect to the diffraction limited value) and a system emissivity SE=(1-optical efficiency) $\simeq 0.5$.

6.1.3. Detector Noise

We consider three types of IR detectors:

Single InSb Detector:

Our group presently operates the IR experiment using a pair of discrete photovoltaic InSb detectors (quantum efficiency $\eta \simeq 80\%$) in combination with a transimpedance pre-amplifier operated in near-zero bias mode. The noise in this system, referred to the op-amp input, arises from op-amp input noise voltage (V_n) and current. We assume the latter to be negligible as we use FET input op-amps. We also consider Johnson noise in the feedback resistor (R_f) and in the real part of the source impedance (R_D). As the different noise sources add in quadrature, the input rms noise current is given by[7]:

$$i_n = \sqrt{4KT\left(\frac{1}{R_D}+\frac{1}{R_f}\right)\Delta f + 4\pi^2 f^2 C_D^2 V_n^2 \Delta f} \tag{35}$$

where C_D represents the detector's capacitance; f is the operating frequency and Δf the noise bandwidth. This electronics is cold and we therefore take the operating temperature to be $T = 50^o K$. We consider two sets of parameters. The first, labelled I, corresponds to our present system and results in noise dominated by the contribution from the pre-amplifier. It is however possible in principle to obtain smaller size (i.e. smaller capacitance) detectors and lower noise op-amps, so that the noise becomes dominated by the Johnson noise contribution; values corresponding to this regime are labelled II and are included in the analysis since they provide a reference as ideal operation of InSb photodiodes:

$InSb_I$:	$InSb_{II}$:
$C_D = 92pF$	$C_D = 10pF$
$V_n = 10nVHz^{-1/2}$	$V_n = 1nVHz^{-1/2}$

where the noise voltage densities are approximately constant over the range of frequencies of interest (0-1KHz). For the resistances, we use the values measured for the present IOTA detectors: $R_f = 2X10^{11}\Omega$ and $R_D = 5X10^{12}\Omega$. The capacitance values correspond to detector sizes of the order $0.5mm$ and $0.2mm$ diameter respectively and have been estimated from Cincinnati Electronics data.

Once the noise current is calculated, we convert to an equivalent number of counts per sample using:

$$\overline{K}_D = \left(\frac{i_n.\delta t}{e}\right)^2, \text{ counts per sample} \tag{36}$$

where e is the electron charge.

NICMOS-3 Array:

The *second generation* IOTA infrared detectors will be based on a NICMOS-3 256X256 HgCdTe (quantum efficiency $\eta \simeq 60\%$) integrating array from Rockwell International Science Center. As previously shown, in this case we have the choice between detecting delay modulated or dispersed fringes, with no fundamental but only practical possible advantages of one technique with respect to the other. The system is currently being designed and assembled and will be available for testing at the site in late 1995. The main source of noise for integrating array detectors is *readout noise*, the rms deviation on the signal read out of a pixel after zero integration time. We assume that readout noise represents a constant noise level per pixel, independent of integration time. We expect to achieve a low level of readout noise in our system of at most ~ 30 electrons rms per pixel. However, in this calculations we allow for a somewhat more conservative value of 50 electrons rms. Further, by performing several multiple non destructive reads per sample it should in principle be possible to reduce this level of read noise by a factor of $\sqrt{N_{reads}}$. These multiple sampling techniques have been demonstrated using an array very similar to ours[3] and it has also been found that this improvement applies for N_{Reads} up to ~ 10, beyond which the noise reduction is not as fast as the inverse square root, and until $N_{Reads} \sim 30$ at which point there is no further improvement, possibly due to pixel glow associated with readout. Our sampling requirements (see later in this paper), together with the limitations in the speed for

addressing and reading out a pixel inherent to the NICMOS-3 chip, will limit the maximum number of multiply correlated measurements per sample to a few tens, still within the range for which significant noise reduction is expected. Therefore, for this system we write:

$$\overline{K}_D = \frac{e_{rms}^2}{N_{reads}}, \text{ counts per sample.} \tag{37}$$

Solid State Photomultiplier:

The third type of detector to be considered (and candidate for our *third generation* detector system) is based on the solid state photomultipliers (SSPM) developed by Rockwell International Science Center.[6] High quantum efficiency photon counting represents the ultimate sensitivity limit and these devices provide the internal gain necessary to achieve photon counting. We will operate the SSPMs in an *edge illuminated* mode in which the photons traverse a longer path of active material ($1000\mu m$, the imaging area being $45X100\mu m$) compared to the *back-illuminated* devices (with a depth of active material of $25\mu m$, the imaging area being $200X200\mu m$), resulting in relatively high levels of quantum efficiency, over 40% at $1-2\mu m$ (to be compared with $2-3\%$ for the back-illuminated devices). The main noise limitation for these detectors comes from *dark current*, which is due to thermal generation of carriers in the active volume of the SSPM. The larger volume of the edge-illuminated device then also results in larger dark count rate. Under optimum operation conditions of voltage bias and temperature the measured dark count rate of the edge-illuminated device is 4000 counts/sec (1500 counts/sec for the back-illuminated). Note however that the factor of ten improvement in quantum efficiency clearly favors the edge-illuminated device. We therefore have in this case:

$$\overline{K}_D = 4000.\delta t, \text{ counts per sample} \tag{38}$$

6.2. Results

Using the standard K band filter there are about 7 fringes within the 1/e width of each interferogram. We need to detect this central fringe packet in one atmospheric coherence time, for which $\tau_0 = 50\ msec$ is a typical value at K. Therefore, imposing a sampling requirement of at least 3 samples per fringe, we obtain a sampling frequency (SF) of 600 Hz (note that $\delta t = SF^{-1}$) and M=21 samples per fringe packet.

Using those parameters in equation (32) of section (5) gives the results summarized in Table 1 for the SNR of fringe visibility for an unresolved source, of $\overline{V}_{object} = 1.0$. We have shown the results corresponding to the NICMOS-3 system for both a basic operation mode of 1 read per sample and a conservative value of 10 reads per sample. To facilitate evaluation of the different detectors, we also show in the table the values of SNR corresponding to photon limited performance, defined as that obtained with zero background and with a perfect detector of 100% quantum efficiency and zero noise.

Note that we base our calculations on a single interferogram since co-adding fringes will only be effective in increasing the SNR (by a factor of $\sqrt{N}$, where N is the number of measurements) if the individual SNRs are higher than ~ 2, since otherwise we incur a significant probability of misidentifying the desired signal. Thus the magnitude limit is set by the ability to detect a single interferogram, but for sources brighter than that limit the uncertainty in the visibility can be reduced by repeated measurements.

From the results summarized in Table 3, we can extract the following conclusions:

- Under ideal Johnson noise limited operation, single InSb detectors can potentially provide a factor of ~ 20 improvement in SNR with respect to our current system.
- That level of performance can be expected to be easily matched by using one or a few pixels of the NICMOS-3 array. Use of multiply correlated sampling is expected to significantly increase the sensitivity given by detector. We also note that in addition to the fact that each array pixel is superior as a detector to the InSb diodes previously considered, the use of arrays offers the possibility, also to be implemented at the IOTA, of using a single chip for both fringe detection and star tracking in the infrared. This represents a crucial advantage with respect to our present configuration in which we are limited to observations of infrared sources which are bright enough visibly to the tracked by our CCD star trackers.

Table 1. Results for $SNR_{\overline{V}}$ at K.

			$NICMOS3$			
m_k	$InSb_I$	$InSb_{II}$	$N_{reads}=1$	$N_{reads}=10$	$SSPM$	$Photon\ Limit$
4	19.7	194.4	150.6	177.6	148.1	237.4
5	7.9	109.9	77.6	106.8	91.6	149.8
6	3.1	56.8	36.1	60.8	55.2	94.5
7	1.2	26.5	15.6	31.6	31.5	59.6
8	0.5	11.4	6.4	14.8	16.4	37.6
9	0.2	4.7	2.6	6.4	7.7	23.7
10	0.08	1.9	1.04	2.7	3.4	14.9

- In the detector noise limited regime, the SSPM are the best devices due to their extremely low noise levels. In the photon rich regime however, they are comparable to the NICMOS-3 device, due to their low quantum efficiency. It is the only device which would allow IOTA observations of IR sources fainter than 10th magnitude.

It is also informative to consider the following Table 2, in which we have calculated the point source limiting magnitude, defined as the value for which we obtain a $SNR_{\overline{V}}=3$, for the three types of detectors. We again include the photon limited value for comparison:

Table 2. Limiting K-magnitudes.

$InSb_I$	$NICMOS3$	$SSPM$	$Photon\ Limit$
6.05	9.8	10.1	14.4

Our immediate upgrade to the NICMOS-3 array will therefore represent a gain of more than 3 magnitudes at K. And about an extra magnitude gain is to be expected from use of the SSPM detectors.

7. APPLICATION TO THE OPTICAL EXPERIMENT

Although the principal motivation of this Report is to evaluate the performance of near-IR detectors, in this section we apply the previous formalism to the two modes of operation at visible wavelengths currently under testing at the IOTA.

For visible light operation at the IOTA, the outputs of the beam splitter are focussed by an array of four lenslets onto multimode optical fibers. Each lenslet has a full aperture referred to the primary of $\simeq 16\ cm$, which corresponds to an r_0 patch at visible wavelengths. The optical fibers are either led to the slit of a grism spectrograph for constant frequency dispersion[4] (dispersed fringes) or directly focussed on the optical detector (delay fringes).

7.1. Noise Sources

7.1.1. Source Photon Noise

Using the standard V-band calibration ($F_o = 3.4x10^{-12} W.cm^{-2}.\mu m^{-1}$), considering a spectral bandwidth of $\simeq 46\%$ centered at $0.65\mu m$ and a system optical efficiency of $\simeq 0.5$; we readily obtain the number of source photocounts in each r_o area as a function of magnitude at V:

$$\overline{K}_S = 3.1X10^8 10^{\frac{-m_v}{2.5}} \eta \delta t \tag{39}$$

which constitutes the signal and gives a shot noise contribution. In the optical case, shot noise from the background photons is negligible.

7.1.2. Detector Noise

Two detectors are considered for optical operation at the IOTA:

CCD:

We consider detection of visible fringes using a thinned, backside illuminated, 512X512 CCD (Scientific Imaging Technologies, Inc.). The device has an average quantum efficiency $\eta \simeq 80\%$ over the considered bandpass and low read noise of 6-12 electrons rms. In this calculation we use a conservative value of 10 electrons rms and the noise contribution is again given by equation (37).

The electronics, cryogenics and optics systems for operation of these detectors is being developed in parallel to the IR NICMOS-3 system and is also expected to be operational in the Fall of 1995.

PAPA Camera:

This is a two-dimensional photon counting detector with 512x512 pixels of resolution and counting rate of $\simeq 200,000/s$.[5] The device has a measured average quantum efficiency over the range of interest of $\simeq 6\%$. In this calculation we consider only photon shot noise for this detector.

7.2. Results

The V-bandpass gives us about 4 fringes in the central lobe of the interferogram, which we wish to detect in one atmospheric coherence time $\tau_0 = 10\ ms$ at V. With our sampling requirement of 3 samples per fringes, we obtain a sampling frequency of 1200 Hz and M=12 samples per fringe packet.

Although in order to match the aperture size to r_o we divide the collecting area in 4 sub-apertures, the 4 independent signals are detected and can be used for further increase in SNR, we therefore use equation (32) multiplied by a factor of $\sqrt{4}$.

The results are summarized in Table 3 for the SNR of fringe visibility for an unresolved object.

Table 3. Results for $SNR_{\overline{V}}$ at V.

	CCD			
m_v	$N_{reads} = 1$	$N_{reads} = 10$	*PAPA*	*Photon Limit*
2	688.05	688.3	188.3	1088.5
4	273.1	273.8	74.9	433.3
6	106.8	108.3	29.8	172.5
8	38.4	41.6	11.9	68.7
10	10.4	13.8	4.7	27.3

REFERENCES

1. Carleton et al., 1994, "Current Status of the IOTA Interferometer", in Proceedings of the SPIE, 2200, 152
2. Dyck, H. M., Benson, J. A., Schloerb, F. P., 1994, "Imaging a Binary Star with a Two-Telescope Michelson Stellar Interferometer",Astronomical Journal, in press
3. Hodapp, K-W., Rayner J., Irwin E., 1992, "The University of Hawaii NICMOS-3 Near-Infrared Camera", P.A.S.P, 104, 441-451
4. Traub, W. A. 1990, J. Opt. Soc. Amer. A, 7, 1779
5. Papaliolios, C., Nisenson, P., Ebstein, S., 1985, "Speckle Imaging with the PAPA detector", Appl. Opt., 24, 287
6. Petrov, M. D., Stapelbroek, M. G., Kleinhans, W. A., 1987, "Detection of Individual $0.4 - 28\mu m$ Wavelength Photons via Impurity-Impact Ionization in a Solid-State Photomultiplier", Appl. Phys. Lett., 51, 406-408
7. Wimmers, J. T., Smith D. S., 1984, "Optimization of Indium Antimonide detectors for use at liquid Helium temperatures", SPIE, 510, 21